Two step mechanism of phosphate release and the mechanism of force generation in chemically skinned fibers of rabbit psoas muscle

Masataka Kawai* and Herbert R. Halvorson‡
*Department of Anatomy, The University of Iowa, Iowa City, Iowa 52242; and ‡Division of Physical Biochemistry, Henry Ford Hospital, Detroit, Michigan 48202 USA

ABSTRACT The elementary steps of contraction in rabbit fast twitch muscle fibers were investigated with particular emphasis on the mechanism of phosphate (Pi) binding/release, the mechanism of force generation, and the relation between them. We monitor the rate constant $2\pi b$ of a macroscopic exponential process (B) by imposing sinusoidal length oscillations. We find that the plot of $2\pi b$ vs. Pi concentration is curved. From this observation we infer that Pi released is a two step phenomenon: an isomerization followed by the actual Pi release. Our results fit well to the kinetic scheme:

Step 2 Step 4 Step 5 Step 6

$$\text{AM*S} \overset{K_2}{\longleftrightarrow} \textit{Det} \underset{k_{-4}}{\overset{k_4}{\rightleftharpoons}} \text{AM*DP} \underset{K_5}{\overset{\text{P}}{\longleftrightarrow}} \text{AM*D} \xrightarrow{k_6}$$

where A = actin, M = myosin, S = MgATP (substrate), D = MgADP, P = phosphate, and *Det* is a composite of all the detached and weakly attached states. For our data to be consistent with this scheme, it is also necessary that step 4 (isomerization) is observed in process (B). By fitting this scheme to our data, we obtained the following kinetic constants: $k_4 = 56\ s^{-1}$, $k_{-4} = 129\ s^{-1}$, and $K_5 = 0.069\ mM^{-1}$, assuming that $K_2 = 4.9$. Experiments were performed at pCa 4.82, pH 7.00, MgATP 5 mM, free ATP 5 mM, ionic strength 200 mM in K propionate medium, and at 20°C. Based on these kinetic constants, we calculated the probability of each cross-bridge state as a function of Pi, and correlated this with the isometric tension. Our results indicate that all attached cross-bridges support equal amount of tension. From this, we infer that the force is generated at step 4. Detailed balance indicates that 50–65% of the free energy available from ATP hydrolysis is transformed to work at this step. For our data to be consistent with the above scheme, step 6 must be the slowest step of the cross-bridge cycle (the rate limiting step). Further, AM*D is a distinctly different state from the AMD state that is formed by adding D to the bathing solution. From our earlier ATP hydrolysis data, we estimated k_6 to be $9\ s^{-1}$.

INTRODUCTION

Transduction of energy by a muscle cross-bridge starts with the binding of MgATP (substrate) to the myosin head, and ends with the release of products. The hydrolysis of ATP takes place while it is bound to the myosin head. Release of products is accelerated in the presence of actin, thus, cross-bridge formation becomes an integral part of the transduction. We visualize the cross-bridge cycle as a steady state which is driven by the availability of substrate and by the system's capacity to absorb products (MgADP, phosphate and mechanical output). The elementary interactions between a cross-bridge state and these molecules are fast on the time scale of the mechanical observations, hence, these interactions can be treated as being at local equilibrium with respect to the kinetic process being studied. Therefore, we anticipate that an increase in the substrate concentration increases the cycling rate, and an increase in the product concentration diminishes the cycling rate. In a previous report, we studied the effect of MgATP and MgADP molecules, and the results substantiate this anticipation (Kawai and Halvorson, 1989*b*).

The role of phosphate in cross-bridge kinetics is of appreciable interest among investigators working on cross-bridge mechanisms of contraction. In biochemical studies it has been shown that about half of the energy available from the hydrolysis of ATP is associated with Pi release (White and Taylor, 1976; Taylor, 1986; Inoue et al., 1989). This observation has led investigators to suggest that the Pi-release step corresponds to the "power stroke" reaction, in which chemical energy available from the hydrolysis of ATP is transduced to mechanical energy to generate force (Huxley, 1980; Hibberd, et al., 1985*a*; Pate and Cooke, 1989). The observation that an increase in Pi concentration reduces isometric tension in skinned fibers (Rüegg et al., 1971; Herzig and Rüegg, 1977; Brandt et al., 1982; Herzig et

0006-3495/91/02/329/14 $2.00

al., 1982; Altringham and Johnston, 1985; Cooke and Pate, 1985; Kawai, 1986; Noske et al., 1987; Bowater and Sleep, 1988; Pate and Cooke, 1989) are consistent with the idea that the Pi-release step is related to the force generating step.

Despite the vast amount of data accumulated on the Pi effect in recent years, a qualitative correlation of isometric tension with the underlying cross-bridge state(s) is scarce. It is essential, for instance, to test whether cross-bridges without Pi support more tension than those which have Pi bound. This lack of critical data may be related to the fact that it is difficult to model the isometric tension in terms of Pi concentration, difficult to find an appropriate kinetic scheme because of multiple steps involved, and difficult to obtain reasonable estimates of necessary kinetic parameters appropriate for the particular experimental conditions. When the scheme is complex, it is often not easy to perform the right simplification of the scheme suitable for explaining experimental observations. The fact that Pi itself may have additional active sites on contractile proteins (Rüegg et al., 1971; White and Thorson, 1972; Bagshaw and Trentham, 1974; Nonomura et al., 1975; Herzig et al., 1982) adds further complications to the problem.

In this report, we assume that the Pi effect is manifested primarily at the Pi-release step, create a simplified cross-bridge scheme that is consistent with the Pi effect on the apparent (observed) rate constant and magnitude parameters, and deduce kinetic parameters. Sinusoidal analysis is particularly useful for studying cross-bridge kinetics because of its high resolving power. In this analysis method, any reaction significantly faster than the frequency of observation can be regarded as being at a local equilibrium (or steady state), whereas any reaction significantly slower than the frequency of observation does not occur in the time frame of the experiment ("kinetic uncoupling;" Hammes, 1968). This significantly simplifies both the kinetic scheme and its algebraic representations. Once the kinetic constants are obtained, we calculate the probability of cross-bridges in each state and its dependence on Pi, and correlate the results with the isometric tension data. Our results indicate that all attached cross-bridges support the same amount of tension regardless of the presence of phosphate. A preliminary account of the present results was presented (Kawai and Halvorson, 1989*a*).

MATERIALS AND METHODS

The source of chemicals and their abbreviations are as reported (Kawai and Halvorson, 1989*b*). The relaxing solution contained (millimolar) 6 EGTA, 2 MgATP, 5 free ATP, 8 Pi (inorganic phosphate), 48 KProp, 62 NaProp, and 10 MOPS. The activating solution in the absence of phosphate contained 6 K_2CaEGTA, 5.34 Na_2MgATP, 4.66 Na_2K_2ATP, 15 Na_2CP, 53.4 KProp, 28.3 NaProp, 10 MOPS, and 160 U/ml CK; 16 Pi solution contained 6 K_2CaEGTA, 5.30 Na_2MgATP, 4.70 Na_2K_2ATP, 15 Na_2CP, 16 KPi, 15.8 KProp, 28.3 NaProp, 10 MOPS, and 160 unit/ml CK. CaEGTA was not included initially in the experimental saline, and it was added at the time of activation. Only two extreme Pi solutions (0 and 16 mM) were prepared initially, and solutions with intermediate concentrations were created by appropriate mixing of the two. The standard activating solution was the same as 8 Pi solution. In all solutions used for experiments, the total Na concentration was maintained at 78 mM, the ionic strength was adjusted to 200 mM with KProp, and pH was adjusted to 7.00 ± 0.01. EGTA, CaEGTA, and Pi were added as neutral K salts; MgATP and CP as neutral Na salts; and free ATP was added as $Na_2K_{1.7}$ATP (a neutral salt). Individual concentrations of multivalent ionic species were calculated using our computer program, which assumed multiple equilibria with the following apparent association constants (log values at pH 7.00): CaEGTA, 6.28; MgEGTA, 1.61; CaATP, 3.70; MgATP, 4.00; CaCP, 1.15; MgCP, 1.30. Our computer calculation showed that pCa of activating solutions was 4.817–4.822, pMg 3.673–3.688, pMgATP 2.301 for different Pi solutions; the experiments were performed at 20.0 ± 0.2°C.

Fiber bundles were dissected from the psoas muscle of New Zealand White rabbits, and skinned in a solution that contained (millimolar) 5 EGTA, 2 MgATP, 5 free ATP, 132 NaProp, and 6 imidazole (pH 7.0) at room temperature (22–25°C) for 10 min. Initial skinning in Na solution (instead of K) and at room temperature (instead of 0°C) dramatically improved the subsequent performance of fibers compared to the original protocol (Eastwood et al., 1979), presumably because these procedures did not induce membrane depolarization, hence, no contraction ensured. An increase in free ATP concentration also helped the integrity of fibers. The improvement was seen by repeating the control activation at the end of a series of experiments, and by observing the integrity of fibers with a high power microscope (below). The bundles were continuously skinned at lower temperature (0–2°C) for 48 h, and stored at −20°C in solution that contained (millimolar) 5 EGTA, 2 MgATP, 5 free ATP, 132 KProp, 6 imidazole (pH 7.0), and 50% (vol/vol) glycerol. Preparations consisting of two fibers were used for experiments reported here. The sarcomere length was adjusted to 2.5 μm by optical diffraction using a He-Ne laser. L_o indicates the length of preparations measured at this time.

Pi study was carried out both in increasing and decreasing orders of Pi concentrations so that any artifact due to the order of experiments would be canceled after averaging. The preparation was monitored by high-power microscope (Leitz, Diavert) throughout the experiments. If any irregularities were noted in the fiber or sarcomere appearance the preparation was discarded. At the beginning and the end of each Pi series experiment, the preparation was tested with the standard activating solution to examine the reproducibility of the data. The data from any preparation which exhibited <80% of the initial tension, bizarre Nyquist plot, or unrealistic rate constants were not used for analysis.

RESULTS

Effect of phosphate on complex modulus

Muscle fibers were activated with a series of solutions of differing phosphate (Pi) concentrations, and complex modulus data $Y(f)$ were collected. Fig. 1 shows the results in Nyquist plots in *A*, and phase shift vs. frequency in *B*. The numbers in the figure indicate the

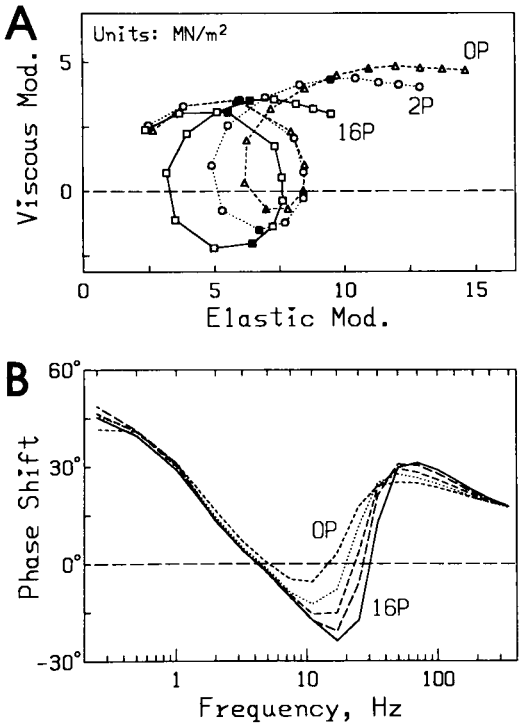

FIGURE 1 Complex moduli are shown in Nyquist plot (*A*) and in phase-frequency plot (*B*) during maximal activation at varying phosphate concentrations as indicated. Averaged results over seven experiments. In *A*, frequencies used are (clockwise): 0.25, 0.5, 1, 2, 3.2, 5, 7.5, 11, 17, 25, 35, 50, 70, 100, 135, 187, 250, and 350 Hz. Decade frequencies (1, 11, 100 Hz) are entered with solid symbols. Only 0, 2, and 16 mM phosphate conditions are shown. Units are meganewtons per square meter in both axes. In *B*, data points are connected with straight lines, and frequencies of observation are indicated across the top of the figure. Only 0 and 16 mM phosphate concentrations are indicated. Other concentrations are 2, 4, and 8 mM in the sequential order. Peak-to-peak amplitude: 0.25% L_o.

millimolar concentrations of Pi. The data reflect averaged results over seven experiments on seven preparations. As seen in the Nyquist plot (Fig. 1 *A*), an increase in Pi concentration noticeably increased the magnitude *B* as represented by an increase in the diameter of the arc which goes through the fourth quadrant. This effect is accompanied by an increase in the characteristic frequency that gives the maximum negative viscous modulus. In Fig. 1 *B*, it is seen that the increase in Pi concentration shifts the minimum position of the phase-frequency plot to the right, indicating that the rate constant $2\pi b$ of process (B) increases with an increase in Pi concentration. The current effect of Pi on the complex modulus in the propionate medium is quantitatively consistent with our earlier study that used chloride medium (Kawai, 1986). The current experiment was performed because of the specific effects of different anions on isometric tension (Andrews et al., 1988, 1989); however, replacing Cl^- with $Prop^-$ did not significantly alter the cross-bridge scheme or the associated kinetic constants under our experimental conditions.

Effect of phosphate on kinetic parameters

The complex modulus data $Y(f)$ were fitted with Eq. 2 of Kawai and Brandt (1980) to extract the rate constant and magnitude parameters, and the averaged results are shown in Fig. 2 ($2\pi b$) and in Fig. 3 (product $2\pi b \cdot B$) for the same experiments as in Fig. 1. The product is shown here, because its analytical form is simpler than that of the magnitude itself (see below). As expected, both quantities increased with an increase in the Pi concentration, with upward bending suggesting that both of them eventually saturate at very high Pi concentrations. The effect of Pi on the rate constant is similar to that on insect muscle (Rüegg et al., 1971; White and Thorson, 1972), cardiac muscle (Herzig and Rüegg, 1977), or rabbit psoas muscle (Hibberd et al., 1985*a*; Kawai, 1986). As noted earlier (Kawai, 1986; Kawai et al., 1987), processes (A) and (C) were much less sensitive to Pi (data not shown). Our primary concern in this report is to account for the large effect of Pi on process (B).

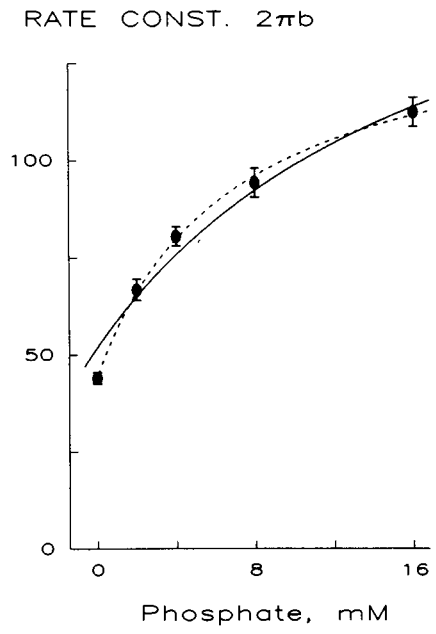

FIGURE 2 Rate constant $2\pi b$ (in s^{-1}) is plotted againt Pi concentration. Circles indicate the average of seven experiments with SEM error bars. Dotted line is the result of fitting the data with Eq. 4. Solid line is the result of simultaneous fitting of the data of Fig. 2 with Eq. 4 and the data of Fig. 3 with Eq. 8 (see text). The best fit parameters are shown in upper half of Table 1.

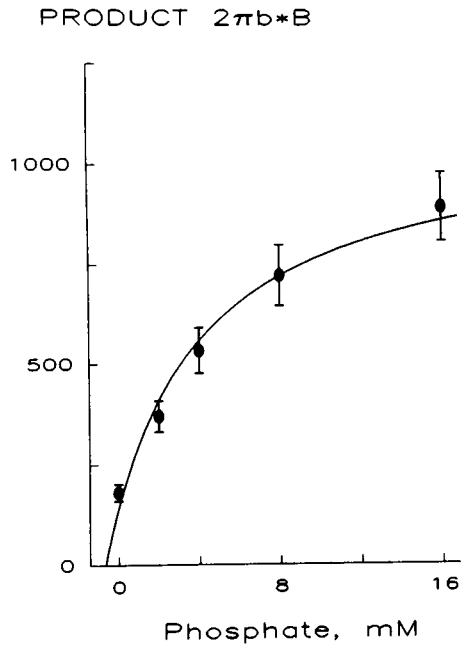

FIGURE 3 The product $2\pi b \cdot B$ (in meganewton per square meter per second) is plotted against Pi concentration. Circles indicate the average of seven experiments with SEM error bars. Solid line is the result of simultaneous fitting of the data of Fig. 2 with Eq. 4 and the data of Fig. 3 with Eq. 8 (see text). The best fit constants are shown in upper half of Table 1.

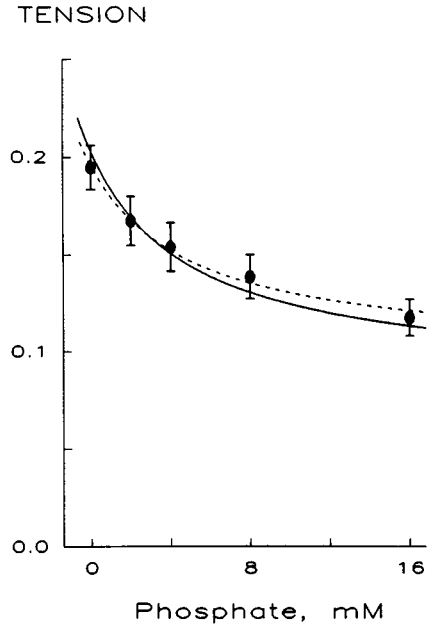

FIGURE 4 Isometric tension is plotted in meganewton per square meter against Pi concentration. Circles indicate the average of seven experiments with SEM error bars. Dotted line is the result of fitting the data with Eq. 9, and solid line is the result of fitting the same data with Eq. 10 (see text).

Effect of phosphate on tension and elastic modulus

Fig. 4 represents isometric tension plotted against Pi concentration for the same experiments. As seen in this figure, the tension decreased gradually with an increase in Pi concentration. The effect is not due to the induction of partial Ca activation because further increase in Ca^{2+} concentration does not induce further tension (Kawai et al., 1981; Brandt et al., 1982). This effect of Pi on isometric tension is consistent with earlier reports on insect muscle fibers (Rüegg et al., 1971), cardiac muscle preparations (Herzig and Rüegg, 1977; Herzig et al., 1982), fish slow twitch fibers (Altringham and Johnston, 1985), and on rabbit psoas fibers (Brandt et al., 1982; Cooke and Pate, 1985; Kawai, 1986; Nosek et al., 1987; Bowater and Sleep, 1988; Pate and Cooke, 1989).

Fig. 5 presents the elastic modulus extrapolated to infinite frequency (Y_∞; defined in Eq. 2 of Kawai et al., 1987) plotted against Pi concentration. This plot is generally similar to the tension vs. Pi plot of Fig. 4: Y_∞ decreases gradually as Pi concentration is increased, indicating that fewer cross-bridges are attached at higher Pi concentrations. The ratio of isometric tension to

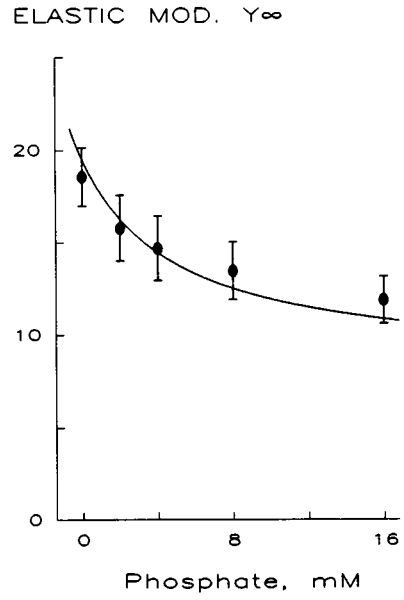

FIGURE 5 Y_∞ (the elastic modulus extrapolated to the infinite frequency) is plotted in meganewton per square meter against Pi concentration. Circles indicate the average of seven experiments with SEM error bars. Solid line is the result of fitting the data with Eq. 11 (see text).

elastic modulus is plotted in Fig. 6 to demonstrate that these quantities have similar dependencies on Pi concentration. This figure shows that the ratio remains approximately the same (1.06 $\%L_o$) as the Pi concentration is changed. The ratio represents the amount of fast length release required to abolish full tension during contraction.

Cross-bridge scheme

The following is the cross-bridge scheme that has been developed from biochemical studies of isolated and reconstituted contractile proteins (Tonomura et al., 1969; Lymn and Taylor, 1971; White and Taylor, 1976; Taylor, 1979, 1986; Stein et al., 1979; Eisenberg and Greene, 1980; Sleep and Hutton, 1980; Inoue et al., 1989) with modification.

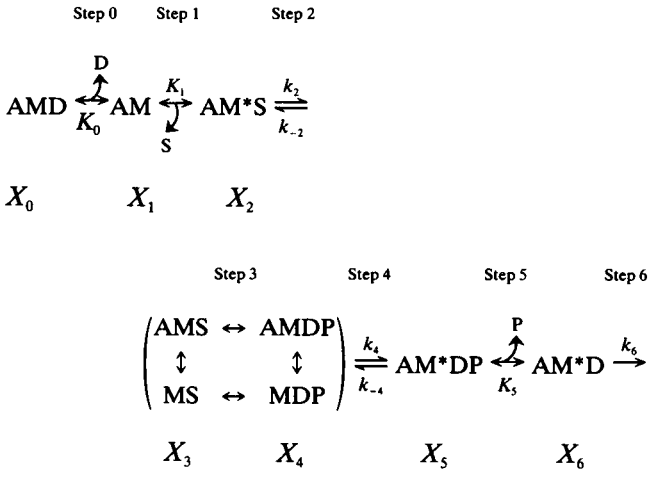

Scheme 3

A = actin, M = myosin head, S = MgATP, D = MgADP, and P = phosphate. An asterisk (*) is placed where a second conformational state is identified or suspected. Also, cross-bridge states (such as M) that are probably not important under physiological conditions are not included. In scheme 3, K_0, K_1, and K_5 are equilibrium association constants for binding of D, S, and P, respectively, to corresponding cross-bridge states. The rate constants k_2 and k_{-2} denote interconversion of step 2, and the rate constants k_4 and k_{-4} denote interconversion of step 4. We previously demonstrated that step 2 was observed in process (C), consistent with MgATP and MgADP effects (Kawai and Halvorson, 1989*b*). In scheme 3, we argue that step 4 is observed in process (B).

In formulating the cross-bridge scheme to explain our results, we used the following approximations and assumptions:

(*a*) Detached states MS and MDP are lumped together in the state *Det.* Because our measurement depends on the attached cross-bridges, it may not be sensitive enough to resolve a subtle difference in the detached states.

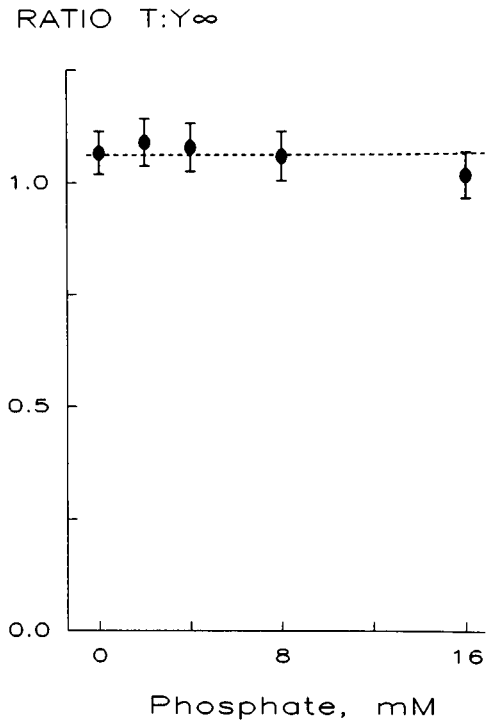

FIGURE 6 Tension:Y_∞ is plotted in $\%L_o$ against Pi concentration. Circles indicate the average of seven experiments with SEM error bars. Dotted line is the average of all the data points.

(*b*) Weakly attached states (Stein et al., 1979; Greene and Eisenberg, 1980) AMS and AMDP are also included in the detached state *Det,* because these cross-bridges are likely to break faster than the speed of the length change we use. In addition, most of the weakly attached cross-bridges dissociate as the ionic strength is raised from 20 to 160 mM (Schoenberg, 1988), hence, their presence in the physiological ionic strength condition (200 mM) may not be significant.

(*c*) The binding of a cross-bridge state with a nucleotide or Pi (step 0, 1, 5) is faster than our detection speed, and is taken as being at steady state. Specifically, the binding reactions are regarded as being sufficiently rapid that they are kinetically uncoupled from process (B). Their influence on process (B) can then be expressed without explicitly considering binding rates. If the binding rates were slow enough to be within the frequency range of the signal, we would observe a linear relationship between concentration and the apparent rate constant. This is contrary to our results for MgATP and MgADP effects on $2\pi c$ (Kawai, 1982; Kawai and

Halvorson, 1989*b*) and Pi effects on $2\pi b$ (Fig. 2), thus substantiating this assumption.

(*d*) The cross-bridge state AM*DP needs to be present. This state is essential to account for the observed curvature of $2\pi b$ vs. Pi plot (Fig. 2). The distinct concave downward curvature means that process (B) is either followed by Pi dissociation (forward reactions of steps 4 and 5) and/or preceded by Pi binding (backward reactions of the same). If process (B) were preceded by Pi dissociation, the curvature would be concave upward (not the case in Fig. 2). The AM*DP state is absent from biochemical schemes, hence, the Pi-release step of solution studies corresponds to the combined steps 4 and 5.

(*e*) Step 6 (the transition from AM*D to AMD or to AM) is the slowest step of the cross-bridge cycle, hence, it can be uncoupled from the rest of scheme 3 based on the principles derived by Hammes (1968) on relaxation kinetics. The validity of this assumption will be examined in the Discussion. We do not know at this time whether the AMD state is on the main hydrolysis pathway.

Simplification of the scheme and algebraic representations

Although it is possible to derive complete algebraic expressions for scheme 3 (see Appendix), the derivations and expressions are complex, obscuring the insight into the problem. Instead, we simplify the scheme to match the experimental conditions. The presence of high concentrations of MgATP (5 mM) together with strong ATP regenerating system (15 mM CP, 160 U/ml CK) justifies elimination of AM and AMD states from the scheme, because the number of cross-bridges in these states is expected to be small (note that $K_1 = 1.4$ mM^{-1}; Kawai and Halvorson, 1989*b*). Another simplification is that if we focus on the frequency range which characterizes step 4, then the faster step 2 can be assumed to be at an equilibrium with the equilibrium constant $K_2 = k_2/k_{-2}$. This approximation is valid, because the rate constant of process (C) is faster than that of process (B). This simplification reduces the number of apparent rate constants from two (scheme 3) to one (scheme 4 below).

$$\text{AM*S} \overset{K_2}{\leftrightarrow} \textit{Det} \underset{k_{-4}}{\overset{k_4}{\rightleftharpoons}} \text{AM*DP} \overset{\text{P}}{\underset{K_5}{\leftrightarrow}} \text{AM*D}$$

Scheme 4

The master equation which describes the kinetics of scheme 4 is:

$$\frac{d}{dt}(\text{AM*S}) + \frac{d}{dt}(Det) = -k_4(Det) + k_{-4}(\text{AM*DP}) = -\frac{d}{dt}(\text{AM*DP}) - \frac{d}{dt}(\text{AM*D}). \quad (1)$$

Because cross-bridges are at the steady state at steps 2 and 5, we approximate these steps with mass action law:

$$(Det) = K_2(\text{AM*S}) \quad (2)$$

$$(\text{AM*DP}) = K_5\text{P}(\text{AM*D}). \quad (3)$$

The expression for the apparent rate constant can be readily developed from Eqs. 1–3:

$$2\pi b = k_4K_2/(1 + K_2) + k_{-4}K_5\text{P}/(1 + K_5\text{P}), \quad (4)$$

under the assumption that P is greater than the myosin concentration (ligand buffering). Eq. 4 can also be derived from the scheme 4 directly by a relaxation kinetics approach as outlined by Hammes (1968). Because K_2 is known from our previous study (Kawai and Halvorson, 1989*b*), values for the kinetic constants k_4, k_{-4}, and K_5 can be obtained by fitting Eq. 4 to the experimental values of $2\pi b$ using the least squares method. An example of such fitting is given as a broken line in Fig. 2. Here we obtain $K_5 = 0.13$ mM^{-1}. However, the fitting is more convincing if it is carried out to satisfy both rate constant and magnitude parameters at the same time, hence, we derive the expression for the magnitude.

Steady-state solutions

To obtain the phosphate dependence of isometric tension and magnitude parameter, the steady-state solution of scheme 4 is needed. This can be derived by setting $K_4 = k_4/k_{-4}$, and $(\text{AM*DP}) = K_4(Det)$. Because the total probability is one:

$$(\text{AM*S}) + (Det) + (\text{AM*DP}) + (\text{AM*D}) = 1. \quad (5)$$

From Eqs. 3 and 5,

$$(\text{AM*DP}) = K_5\text{P}/[1 + \epsilon K_5\text{P}] \quad (6)$$

$$(\text{AM*D}) = 1/[1 + \epsilon K_5\text{P}], \quad (7)$$

where $\epsilon = 1 + (1 + K_2)/K_2K_4$. Note that $(Det) = (\text{AM*DP})/K_4$ and $(\text{AM*S}) = (\text{AM*DP})/K_2K_4$ for the steady-state condition. These can be readily derived from Eq. 6, and exhibit the same phosphate dependence as (AM*DP). From Eqs. 6 and 7, it is evident that (AM*S), (*Det*), and (AM*DP) are increasing functions of P, whereas (AM*D) is a decreasing function of P.

Product, instead of magnitude parameter

It is more convenient to derive an expression for the product of the apparent rate constant and the associated magnitude parameter, than the magnitude parameter itself:

$$2\pi b \cdot B = B_0 k_4 (Det) = B_0 k_{-4} (\text{AM*DP}) = B_0 k_{-4} K_5 \text{P}/[1 + \epsilon K_5 \text{P}]. \quad (8)$$

The proportionality constant B_0 depends on the cross-bridge's sensitivity to the applied length change. Note that the product represents the amount of oscillatory work (Eq. 1 of Kawai, 1986).

Data fitting and kinetic constants

To find kinetic constants k_4, k_{-4}, and K_5, which specify the scheme 4, the data in Figs. 2 and 3 were simultaneously fitted with Eqs. 4 and 8 to minimize the sum of squares. Because the product in Fig. 3 is generally 10 times larger than the rate constant in Fig. 2, 10 times less weight was given for the product than the rate constant in performing the simultaneous fitting. During the fitting, it was noticed that the product plot had a negative intercept on the ordinate (Fig. 3), which is not explained by Eq. 8. Thus, we introduced an additional parameter P_0 and replaced P with P + P_0 in all equations. This parameter P_0 would specify the average phosphate concentration in the muscle preparation when no exogenous phosphate is added. The results from each preparation were fitted first (5 × 2 points), and individual constants were averaged for seven experiments. These results are listed in Table 1. The pooled data (35 × 2 points) were also fitted. The resulting theoretical projections are plotted in Figs. 2 and 3 with solid lines. The best fit constants are listed in Table 1. As seen in these figures, the agreement between the experiment and the theoretical projection is generally satisfactory. As is seen in Table 1, SEM of the kinetic constants are in the range of 4–11%, exhibiting a good reproducibility of the rate constant results among different preparations. This demonstrates the high resolving power of our sinusoidal analysis technique, which could not be achieved in the time domain analysis.

Based on the kinetic constants thus determined, probabilities of all cross-bridge states were calculated from Eqs. 6 and 7, and plotted in Fig. 7 as functions of Pi concentration. Also included in Fig. 7 is the probability of AM, which is calculated from one of Eqs. 18 based on [MgATP] = 5 mM and K_1 = 1.4 mM^{-1} (Kawai and Halvorson, 1989*b*). As shown in this figure, the probability of a cross-bridge in state AM is 1.2% at our standard activating conditions, and justifies the approximation of scheme 4.

TABLE 1 **Kinetic constants which specify schemes 3 and 4**

Constant	Best fit	Average	Units
k_4	56.4	56 ± 2	s^{-1}
k_{-4}	135	129 ± 10	s^{-1}
$K_4 = k_4/k_{-4}$	0.419	0.45 ± 0.05	
K_5	0.059	0.069 ± 0.007	mM^{-1}
$K_5 k_{-4}$	7.97	8.9 ± 0.9	$mM^{-1}s^{-1}$
k_6*	—	9.0	s^{-1}
P_0	0.647	0.62 ± 0.08	mM
B_0	31.2	32 ± 3	MNm^{-2}
T_5	0.377	0.37 ± 0.03	MNm^{-2}
T_6	0.211	0.21 ± 0.01	MNm^{-2}
T_a	0.221	0.22 ± 0.01	MNm^{-2}
Y_a	21.2	21 ± 2	MNm^{-2}
T_a/Y_a	1.062	1.06 ± 0.05	$\%L_o$

*Based on ATP hydrolysis rate measurement (Kawai et al., 1987). The best fit data were obtained after fitting all the available data with Eqs. 4, 8–11, and used for calculation of theoretical curves in Figs. 2–7. The average and SEM (shown in ±) indicate the average of individual data fitting for seven experiments. MN = meganewtons. K_2 = 4.9 is assumed.

Isometric tension

It has been hypothesized that tension develops when phosphate is released from the myosin head after it is attached to actin (see Discussion): AM*D would seem to be a prime candidate for the "tension" state. The fact that isometric tension declines with an increase in P (Fig. 4) and that AM*D is a decreasing function of P (Eq. 7) appear to be in accord with this hypothesis. However, our initial efforts to fit the isometric tension to Eq. 7 failed in all cases we examined, because Eq. 7 declines far more steeply with P than does the observed isometric tension (compare the theoretical projection of AM*D in Fig. 7 with actual tension data in Fig. 4). To circumvent this problem, we tested two hypotheses. In one we assumed that the isometric tension is a linear combination of AM*DP and AM*D states:

$$\text{Tension} = T_5(\text{AM*DP}) + T_6(\text{AM*D}) = (T_5 K_5 \text{P} + T_6)/[1 + \epsilon K_5 \text{P}]. \quad (9)$$

Note that, with this hypothesis, the tension supported by the AM*S state is zero. In the second hypothesis, we assumed that the tension is supported by all attached cross-bridges equally:

$$\text{Tension} = T_a [(\text{AM*S}) + (\text{AM*DP}) + (\text{AM*D})] = T_a [1 + (1 + 1/K_2 k_4)]/[1 + \epsilon K_5 \text{P}]. \quad (10)$$

On fitting the isometric tension data with Eq. 9 or 10, we used the kinetic constants as shown in the upper half of Table 1, replaced P with P + P_0 in Eqs. 9 and 10, and minimized the sum of squares to find linear coefficients T_5 and T_6, or T_a. The results are listed in the lower half of Table 1. These numbers indicate the amount of tension cross-bridges can support if they are 100% in the respective state. The dotted line in Fig. 4 represents the theoretical projection based on Eq. 9 with T_5 and T_6. The solid line represents the theoretical projection based on Eq. 10 and T_a. As shown in this figure, the fitting is satisfactory in either direction. Eq. 9 appears to fit better than Eq. 10, because Eq. 9 utilizes two coefficients instead of one. If the assumptions of Eq. 9 are correct, T_5 = 0.38 MN/m^2 and T_6 = 0.21 MN/m^2 (Table 1) indicate that a cross-bridge in the AM*DP state supports 1.8 times more tension than when in the AM*D state. If the assumptions of Eq. 10 are correct, T_a = 0.22 MN/m^2 indicates that all attached cross-bridge states support the same amount of tension, which corresponds to 0.22 MN/m^2 (when 100% attached).

Elastic modulus Y_∞

The elastic modulus obtained by extrapolation to infinite frequency is proportional to the number of attached cross-bridges:

$$Y_\infty = Y_a[(AM^*S) + (AM^*DP) + (AM^*D)]$$
$$= Y_a[1 + (1 + 1/K_2k_4)]/[1 + \epsilon K_5 P], \quad (11)$$

where Y_a represents the elastic modulus when all cross-bridges are attached. The results of fitting Y_∞ with Eq. 11 are shown in Fig. 5. The fitting is satisfactory and we obtained Y_a = 21 MN/m^2 on the average (Table 1). From Eqs. 10 and 11, Tension/Y_∞ = T_a/Y_a, and this is represented by a dotted line in Fig. 6.

DISCUSSION

Effect of phosphate on exponential process (B)

The most important finding in the current study is that an increase in phosphate (Pi) concentration results in an increase in both the rate constant $2\pi b$ and the product $2\pi b \cdot B$ of process (B) in agreement with the predictions of Eqs. 4 and 8 (Figs. 2 and 3). This finding indicates that scheme 4 is a close approximation to the events taking place in skinned fibers. Because we showed that scheme 1 follows the effects of MgATP and MgADP (Kawai and Halvorson, 1989*b*), and scheme 4 is an abbreviated form of scheme 3 under the present experimental conditions, we can conclude that combined scheme 3 is consistent with the effects of MgATP, MgADP, and Pi.

The presence of the AM*DP state is essential to account for the curvature of the data in Fig. 2. This state was not previously recognized in the scheme based on solution studies (Tonomura et al., 1969; Lymn and Taylor, 1971; Taylor, 1979, 1986; Stein et al., 1979; Eisenberg and Greene, 1980; Inoue et al., 1989). Its presence was assumed to account for the data from glycerinated insect flight muscles (Molloy et al., 1987), and for rabbit psoas muscles (Nagano and Yanagida, 1984; Homsher and Millar, 1990). Therefore, the Pi-release step discussed by biochemists must be understood to be the combined steps 4 and 5 in terms of the scheme 3.

The fact that we have to add P_0 (= 0.6 mM) to P is reasonable when we realize that phosphate concentration is higher in the interior of a fiber, because ATP is continuously hydrolyzed to generate Pi, which then diffuses out from the fiber under a concentration gradient. This situation has been analyzed by Pate and Cooke (1989) for a fiber with a diameter of 70 μm and in the presence of sucrose and sucrose kinase which diminish the Pi gradient. They calculated that, on average, a 0.2 mM difference in Pi exists between the fiber and the solution. Because we did not employ sucrose and sucrose kinase, our estimate of 0.6 mM is reasonable in terms of Pate and Cooke's calculation.

Effect of phosphate on tension

The fact that isometric tension declines with an increase in Pi concentration (Fig. 4) is consistent with the idea that AM*D state is a tension state, because no other cross-bridge state in scheme 3 or 4 has this property (Eqs. 6, 7, 18). In solution studies, the Pi release accompanies a large free energy reduction corresponding to 1/2 of the energy available in ATP hydrolysis (White and Taylor, 1976; Taylor, 1986; Inoue et al., 1989). Because of this, the Pi-release step is generally considered to be the "power stroke" reaction that results in force generation (Huxley, 1980; Hibberd et al., 1985*a*; Pate and Cooke, 1989). Hence, one would expect AM*DP to be the pretension or low tension state, and that Eq. 7 would satisfy the observed isometric tension data after proper scaling.

On the contrary, our effort to fit the experimental isometric tension in Fig. 4 with Eq. 7 failed in all cases: with the equilibrium constants in Table 1, the phosphate dependence of AM*D is a steeply falling function as shown in Fig. 7, and it does not explain the observed tension data. We thus hypothesized two cases on cross-bridge states which support isometric tension: one assumes a linear combination of AM*DP and AM*D (Eq.

9), the other assumes all attached cross-bridges support the same amount of tension (Eq. 10).

The result of the data fitting is satisfactory for both cases. However, in the case of the first hypothesis, we find $T_5 = 0.37$ MNm^{-2} and $T_6 = 0.21$ MNm^{-2}, indicating that a cross-bridge in the AM*DP state has to support 1.8 times more tension than when in the AM*D state, hence, a decline of tension (43%) must accompany with the Pi release. Such a system would be inefficient, because this 43% is probably lost before a cross-bridge has a chance to perform external work. In the second hypothesis, all strongly attached cross-bridges support the same amount of tension, regardless of the specific attached state. We find the corresponding tension to be 0.22 MNm^{-2} when 100% attached (Table 1). This system is more efficient because there is enough time for cross-bridges to perform external work as they proceed steps 5, 6, 0, 1, that include the rate limiting step (see below). In either case, the state AM has to support the equivalent amount of tension as the state AM*D, else the MgATP dependence of isometric tension (Fig. 4 of Kawai and Halvorson, 1989*b*) cannot be explained. From the above reasons, we conclude that the second hypothesis is more likely to be the case, although we could not completely rule out the first hypothesis with the present experiments.

Another possibility is to assume that force is supported by the AM and AM*S states in addition to AM*D, and not by AM*DP. However, the number of cross-bridges in states AM and AM*S is small (9% in all, Fig. 7) in our standard activating conditions (5 mM MgATP, 8 mM Pi), hence, a cross-bridge in these states has to support 3.6 times more tension than that in AM*D, an unlikely outcome. We know from experiments with rigor fibers that a cross-bridge in rigor state can support up to the same amount of tension as an actively cycling one, but not more (Kawai, 1986).

Force generation and phosphate release steps

Based on the above conclusion, we state that the force generation takes place in step 4, and not in step 5 (actual Pi release). If the weakly attached cross-bridges, that are shown to be present in relaxed muscles at low ionic strength (Nagano and Yanagida, 1984; Schoenberg, 1988), are present in activated muscle at physiological ionic strength (200 mM), then it follows that the weak-to-strong transition (AMDP → AM*DP in scheme 3) generates force, and that this transition is an isomerization reaction. If, however, the weakly attached cross-bridges are not present under our experimental conditions, then it follows that the cross-bridge attachment reaction (MDP → AM*DP) generates force. In either case, Pi is retained on the myosin head while the force is being generated. Thus, it can be concluded that the biochemically identified Pi-release step actually consists of two steps with our skinned fiber experiments. In this mechanism, the force generation occurs first, then followed by Pi release which presumably stabilizes the force generating complex. A similar mechanism was suggested by Nagano and Yanagida (1984) and Homsher and Millar (1990) on rabbit psoas muscles, by Molloy et al. (1987) on insect *Lethocerus* muscles, and by Brozovich et al. (1988) on frog skeletal muscle fibers. In fact, our forward and backward rate constants for isomerization (56 s^{-1} and 129 s^{-1}, respectively) closely correlate with those (80 s^{-1} and 130 s^{-1}, respectively) of Homsher measured by use of caged Pi on rabbit psoas at 20°C (Homsher, personal communication).

Our earlier observation, that process (B) is modified by Ca^{2+} concentration (Kawai et al., 1981; Kawai, 1982), is consistent with the idea that the isomerization step 4 is controlled by Ca via troponin-tropomyosin system (Ebashi and Endo, 1968), and that the actual Pi-release step 5 is not Ca sensitive. This insight does not contradict the conclusion of Chalovich and Eisenberg (1982), who found in solution studies that the Pi-release step was controlled by Ca, assuming that steps 4 and 5 were combined in these biochemical experiments. Our earlier results indicate that the Ca control is in an all-or-none manner, and that the rate constant is not altered by the Ca^{2+} concentration.

From our value of the association constant of Pi to AM*DP ($K_5 = 0.069$ mM^{-1}, Table 1), the dissociation constant is calculated to be 14 mM. Our value is lower (8 mM) if we use only the rate constant data for fitting (Fig. 2, *dashed line*). These values compare with ~10 mM based on shortening velocity (Cooke and Pate, 1985), ~5 mM based on caged Pi experiments (Homsher, personal communication), and with the $K_m = 3$ mM based on ^{18}O exchange rate (Bowater and Sleep, 1988), all in skinned psoas fibers. The corresponding value obtained from solution studies is on the order of 1–10 M (Taylor, 1986) for the dissociation of the acto-S1.ADP.Pi state, presumably because this includes the isomerization step (step 4). Thus, one may conclude that the association of Pi with the myosin head takes place at low millimolar concentrations in skinned fibers, whereas the reversal of the Pi-release step is almost impossible in solution studies. Our composite second order rate constant for Pi binding (K_5k_{-4}) is 8.9 mM^{-1}s^{-1}, which is similar to our earlier value (10 mM^{-1}s^{-1}; Kawai et al., 1987); these are consistent with values (1.5–10 mM^{-1}s^{-1}) that Goldman and his colleagues found in skinned fibers by using photolysis of caged ATP (Goldman, 1987).

The above mechanism of force generation in skinned fibers explains the ease of exchange of the phosphate

group with that bound to a nucleotide-myosin complex (Ulbrich and Rüegg, 1971, 1977; Gillis and Marechal, 1974; Hibbard et al., 1985*b*), because at step 4 the free energy is retained as the potential energy (= force) in the compliant portion of cross-bridges, and because a large free energy reduction need not take place with the Pi release (step 5). More recently, Bowater and Sleep (1988) observed that ^{18}O exchange is 500 times faster in skinned fibers than in isolated acto-S1 (S1 = myosin subfragment one), an observation that is consistent with our conclusion.

Populations of cross-bridges in attached states

The result of fitting the elastic modulus (Y_∞) with Eq. 11 is generally satisfactory when the phosphate concentration is changed (Fig. 5). This indicates that scheme 4 and Eq. 11 produce a good approximation in terms of the number of attached cross-bridges. Furthermore, our conclusion that all attached cross-bridges (excluding the weakly attached ones) contribute equally to both tension and Y_∞ is another way of stating that the ratio Tension:Y_∞ is a constant and independent of Pi concentration. Fig. 6 clearly demonstrates this point, and we obtained the ratio 1.06 $\%L_0$ (Table 1).

As shown in Fig. 7, the probability of cross-bridges in states AM, AM*S, *Det*, AM*DP, and AM*D is 1, 8, 41, 18, and 32%, respectively, for our standard activating conditions. This cross-bridge distribution shows that 59% of cross-bridges are in attached states, and 41% in the detached state. This agrees with our earlier estimates of the attached cross-bridge numbers during the standard activation. We reported that 57 ± 10% (1 SD, $N = 7$) are attached to thin filaments by comparing Y_∞ of activated fibers and the elastic modulus of rigor fibers (Kawai, 1982). From the constants given by Schoenberg (1988), we estimate the probability of cross-bridges in the weakly attached state to be 2%, and that of truly dissociated cross-bridges to be 39%.

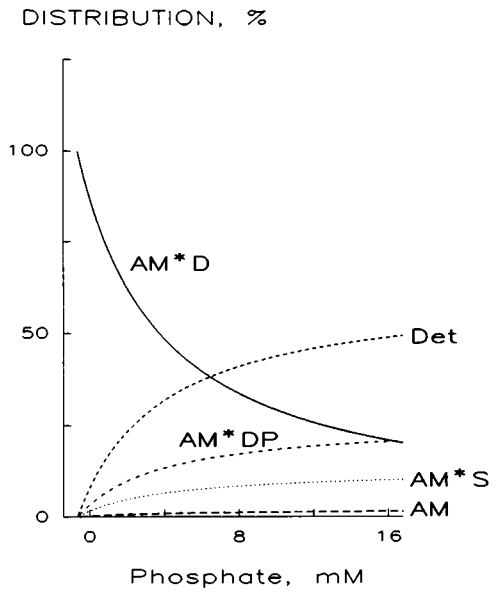

FIGURE 7 The steady-state probability (in percent) of cross-bridge states are plotted against Pi concentration. These are based on Eqs. 6, 7, and 18 with best fit parameters in Table 1 and published constants (see text).

Two AMD states and the rate limiting step

The next questions are whether the AM*D state and the AMD state are identical, and whether step 6 is required to account for our data. If the AM*D and AMD states are identical, Eqs. 1–11 must be rewritten to include this fact. An analysis of such a kinetic scheme shows that step 2 is no longer isolated from step 5, predicting Pi effects on both rate constants $2\pi b$ and $2\pi c$ in a manner not consistent with our observations. Thus, we can rule out such possibility. In another words, AM*D and AMD are two distinctly different cross-bridge states. This important conclusion on skinned fibers is consistent with the results on isolated acto-S1 system as reported by Sleep and Hutton (1980). They showed that an acto-S1 complex which has bound exogenous ADP is energetically distinct from the acto-S1-ADP complex that is produced as a result of the hydrolysis of ATP.

There is only one way to close scheme 3 without altering Eqs. 1–11 or the Pi effects they predict. This is to add a slow step 6: AM*D → AMD or AM*D → AM. The step must be at least several times slower than $2\pi b$ for the above equations not to be affected. In other words, step 6 is the rate limiting reaction (limits the ATP hydrolysis rate), substantiating our assumption that step 6 is the slowest step in the cross-bridge cycle. In comparison, Hibberd et al. (1985*a*) concluded that either the phosphate or the ADP release step is the rate limiting step in isometrically contracting psoas fibers. Siemankowski et al. (1985) suggested that the ADP dissociation rate limits the shortening velocity in psoas. Lund et al. (1987) concluded that the Pi release step is the rate limiting step in insect *Lethocerus* fibers. Mechanisms for the Pi-release step may differ for *Lethocerus* fibers and rabbit psoas fibers.

The rate constant for step 6 can be estimated from the ATP hydrolysis rate. The turn over number based on such measurements is on the order of 1 mol ATP s^{-1} per myosin head (Curtin et al., 1974; Levy et al., 1976; Arata et al., 1977; Takashi and Putnam, 1979; Ferenczi et al.,

1984; Glyn and Sleep, 1985). We recently observed the ATP hydrolysis rate and estimated the turn over number to be 3 mol ATP s^{-1} per myosin head (Kawai et al., 1987) in conditions similar to the current experiments. Thus, we calculate $k_6 = 3/0.32 = 9\ s^{-1}$ for step 6, because 32% of the cross-bridges are in the AM*D state under our standard activating conditions. Actual value for k_6 would be smaller than this, because of the possibility of multiple hydrolysis pathways. In comparison, Taylor (1979) calculated the rate of product release from acto-S1.ADP.Pi to be 4.5 s^{-1}. A close agreement can be seen between skinned fibers and solution studies.

Detailed balance

Because one mole of MgATP is hydrolyzed as the cross-bridge cycle proceeds from left to right in scheme 3, the combined overall free energy change (ΔG) must equal that of ATP hydrolysis:

$$\Delta G = -W + RT \ln (K),$$

where

$$K = K_0 D \cdot K_5 P / K_1 S K_2 K_4 K_6$$

W represents work performed, R the gas constant, T absolute temperature, and $-RT \cdot \ln (K)$ heat generation. If we assume that D = 0.02 mM (estimate), S = 5 mM, P = 8 mM, and $K_6 = 50$, then $K = 4 \times 10^{-5}$ will result with the equilibrium constants listed in Table 1 and $K_0 = 2.8\ mM^{-1}$, $K_1 = 1.4\ mM^{-1}$, $K_2 = 4.9$ (Kawai and Halvorson, 1989*b*). MgATP (S) and Pi concentrations are those of our standard activating conditions, and K_6 is the value estimated by Sleep and Hutton (1980). If we set $\Delta G = -50$ kJ/mol (free energy change for ATP hydrolysis; Kushmerick and Davies, 1969), $W = -\Delta G + RT \ln (K) = 50 - 25 = 25$ kJ/mol will result. Similarly, if we set $\Delta G = -72$ kJ/mol (Meyer et al., 1985), $W = 47$ kJ/mol will result. This means that 25 kJ/mol is lost as heat along the hydrolysis pathway, and that 25 to 47 kJ/mol (50–65%) is made available for stretching the elastic portion of the cross-bridges (i.e., tension generation) at step 4. Actual efficiency would be smaller than this calculation, because the tension is lost with the detachment of cross-bridges. The combined free energy change from steps 4 and 5 is:

$$\Delta G_{4+5} = -W + RT \ln (K_5 P / K_4).$$

Because $K_5 P / K_4 \sim 1$ (Table 1), the combined free energy change for steps 4 and 5 is also −25 to −47 kJ/mol. This combined energy change may correspond to the large free energy reduction associated with the Pi-release step observed in solution studies (White and Taylor, 1976; Taylor, 1986; Inoue et al., 1989), because the biochemical studies did not consider the presence of the AM*DP state.

We initiated this study to develop a cross-bridge scheme for the skinned fiber system, independent of the schemes developed from biochemical studies on isolated proteins. Our results indicate that the scheme thus developed closely parallels those known from biochemical studies: some kinetic constants are shown to be similar to both systems, whereas others are shown to be different. Our analysis further indicates that an additional attached cross-bridge state AM*DP is required to account for the phosphate effect, and that the isomerization step to form the AM*DP state generates force. These studies are essential in determining the molecular events that are controlled by the imposed length changes, and in finding the mechanisms that couple ATP hydrolysis to force generation.

APPENDIX

In the following, a complete algebraic representation of cross-bridge scheme 3 is given. The master equations which govern this scheme are given by:

$$\begin{aligned} \dot{X}_0 + \dot{X}_1 + \dot{X}_2 &= -k_2 X_2 + k_{-2} X_{34} \\ \dot{X}_{34} &= k_2 X_2 - k_{-2} X_{34} - k_4 X_{34} + k_{-4} X_5 \\ \dot{X}_5 + \dot{X}_6 &= k_4 X_{34} - k_{-4} X_5, \end{aligned} \tag{12}$$

where $X_0, X_1, X_2, X_{34}, X_5$, and X_6 indicate the probability of cross-bridges in states AMD, AM, AM*S, *Det*, AM*DP, and AM*D, respectively. A dot ($\cdot$) above a cross-bridge state indicates d/dt. Because k_6 is the slowest step, it does not affect any of the observed processes. Because steps 0, 1, and 5 are in rapid equilibria, $X_0 = K_0 D X_1$, $X_2 = K_1 S X_1$, $X_5 = K_5 P X_6$ can be assumed. From these, Eqs. 12 can be rearranged in a matrix equation:

$$\frac{\mathrm{d}}{\mathrm{d}t} \begin{pmatrix} X_2 \\ X_{34} \\ X_5 \end{pmatrix} = \begin{pmatrix} -\gamma k_2 & \gamma k_{-2} & 0 \\ k_2 & -(k_{-2} + k_4) & k_{-4} \\ 0 & \zeta k_4 & -k_{-4} \end{pmatrix} \begin{pmatrix} X_2 \\ X_{34} \\ X_5 \end{pmatrix}, \tag{13}$$

where

$$\gamma = K_1 S / (1 + K_0 D + K_1 S);\ \zeta = K_5 P / (1 + K_5 P).$$

The apparent (= observed) rate constants of scheme 3 are given by the negatives of Eigen values of the 3 × 3 matrix in Eq. 13, and they are the roots of the following cubic equation:

$$r^3 - (\gamma k_2 + k_{-2} + k_4 + \zeta k_{-4}) r^2 + (\gamma k_2 k_4 + \zeta k_{-2} k_{-4} + \gamma \zeta k_2 k_{-4}) r = 0.$$

Therefore,

$$r_2 + r_3 = \gamma k_2 + k_{-2} + k_4 + \zeta k_{-4} \tag{14}$$

$$r_2 \cdot r_3 = \gamma k_2 k_4 + \zeta k_{-2} k_{-4} + \gamma \zeta k_2 k_{-4}, \tag{15}$$

for two apparent rate constants r_2 and r_3. Note $r_1 = 0$, and this root

provides the constant term. The results of S, D, and P effects on r_2 and r_3 can be fitted with Eqs. 14 and 15 simultaneously to obtain all seven kinetic constants. If the rate constants are sufficiently different, such that $r_2 \gg r_3$ and $\gamma k_2 + k_{-2} \gg k_4 + \zeta k_{-4}$, then Eqs. 14 and 15 can be rewritten as:

$$r_2 = \gamma k_2 + k_{-2} = \frac{K_1 S}{1 + K_0 D + K_1 S} k_2 + k_{-2} = 2\pi c \quad (16)$$

$$r_3 = \frac{\gamma K_2}{\gamma K_2 + 1} k_4 + \zeta k_{-4}$$

$$= \frac{K_2 K_1 S}{1 + K_0 D + (1 + K_2) K_1 S} k_4 + \frac{K_5 P}{1 + K_5 P} k_{-4} = 2\pi b, \quad (17)$$

r_2 in Eq. 16 is the form obtained in our earlier paper for $2\pi c$ (Kawai and Halvorson, 1989*b*), and r_3 in Eq. 17 is a general expression for $2\pi b$ which includes the effects of S, D, and P. Eq. 17 reduces to Eq. 4 for $D \to 0$ and $S \to \infty$. It is important to note that Eqs. 16 and 17 show that an apparent rate constant is a linear combination of the forward and backward rate constants of underlying elementary reaction with positive coefficients. Eqs. 16 and 17 can also be derived from the relaxation kinetics approach directly from scheme 3 as outlined by Hammes (1968).

Steady-state solutions can be obtained by setting

$$X_0 + X_1 + X_2 + X_{34} + X_5 + X_6 = 1,$$

and by setting Eq. 12 to be zero ($X_5 = K_4 X_{34}$, $X_{34} = K_2 X_2$). From these,

$$\begin{aligned} X_0 &= K_0 D K_5 P/M \\ X_1 &= K_5 P/M \\ X_2 &= K_1 S K_5 P/M \\ X_{34} &= K_1 S K_2 K_5 P/M \\ X_5 &= K_1 S K_2 K_4 K_5 P/M \\ X_6 &= K_1 S K_2 K_4/M, \end{aligned} \quad (18)$$

where

$$M = [1 + K_0 D + K_1 S(1 + K_2 + K_2 K_4)] K_5 P + K_1 S K_2 K_4.$$

Products (= rate constant X magnitude) are given by:

$$2\pi b \cdot B = B_0 k_4 X_{34} = B_0 k_4 K_1 S K_2 K_5 P/M \quad (19)$$

$$2\pi c \cdot C = C_0 k_2 X_2 = C_0 k_2 K_1 S K_5 P/M. \quad (20)$$

If isometric tension and the elastic modulus extrapolated to the infinite frequency (Y_∞) are supported by all attached cross-bridges (AMD, AM, AM*S, AM*DP, AM*D) equally, then

$$\text{Tension}/Y_\infty = T_a/Y_a \quad (21)$$

$$\begin{aligned} \text{Tension} &= T_a(X_0 + X_1 + X_2 + X_5 + X_6) \\ &= T_a\{[1 + K_0 D + K_1 S(1 + K_2 K_4)] K_5 P \\ &\quad + K_1 S K_2 K_4\}/M. \end{aligned} \quad (22)$$

The authors would like to thank Mr. Richard W. Arbuckle and Mr. Michael P. Noel for their technical assistance.

The present work was supported by grants from National Institutes of Health (AR21530 to Masataka Kawai; GM23302 to Herbert R. Halvorson) and the American Heart Association (AHA) (88-0727 to Masataka Kawai). Masataka Kawai was an established investigator of AHA.

Received for publication 12 February 1990 and in final form 4 October 1990.

REFERENCES

Altringham, J. D., and I. A. Johnston. 1985. Effects of phosphate on the contraction properties of fast and slow muscle fibres from an antarctic fish. *J. Physiol. (Lond.).* 368:491–500.

Andrews, M. A., T. A. Nosek, and R. E. Godt. 1988. Ion-man competition: in search of the best salt for adjusting ionic strength in skinned skeletal muscle experiments. *Biophys. J.* 53:570a. (Abstr.)

Andrews, M. A., D. W. Maughan, and R. E. Godt. 1989. Warning: certain anions may be hazardous to your skinned rabbit psoas muscle fibers. *Biophys. J.* 55:266a. (Abstr.)

Arata, T., Y. Mukohata, and Y. Tonomura. 1977. Structure and function of the two heads of the myosin molecule. VI. ATP hydrolysis, shortening, and tension development of myofibrils. *J. Biochem. (Tokyo).* 82:801–812.

Bagshaw, C. R., and D. R. Trentham. 1974. The characterization of myosin-product complexes and of product-release steps during the magnesium ion-dependent adenosine triphosphatase reaction. *Biochem. J.* 141:331–349.

Bowater, R., and J. Sleep. 1988. Demembranated muscle fibres catalyze a more rapid exchange between phosphate and adenosine triphosphate than actomyosin subfragment 1. *Biochemistry.* 27:5314–5323.

Brandt, P. W., R. N. Cox, M. Kawai, and T. Robinson. 1982. Regulation of tension in skinned muscle fibers: effect of cross-bridge rate constants on apparent Ca sensitivity. *J. Gen. Physiol.* 79:997–1016.

Brozovich, F. V., L. D. Yates, and A. M. Gordon. 1988. Muscle force and stiffness during activation and relaxation. *J. Gen. Physiol.* 91:399–420.

Chalovich, J. M., and E. Eisenberg. 1982. Inhibition of actomyosin ATPase activity by troponin-tropomyosin without blocking the binding of myosin to actin. *J. Biol. Chem.* 257:2432–2437.

Cooke, R., and E. Pate. 1985. The effect of ADP and phosphate on the contraction of muscle fibers. *Biophys. J.* 48:789–798.

Curtin, N. A., C. Gilbert, K. M. Kretzschmar, and D. R. Wilkie. 1974. The effect of the performance of work on total energy output and metabolism during muscular contraction. *J. Physiol. (Lond.).* 238:455–472.

Eastwood, A. B., D. S. Wood, K. L. Bock, and M. M. Sorenson. 1979. Chemically skinned mammalian skeletal muscle. I. The structure of skinned rabbit psoas. *Tissue and Cell.* 11:553–566.

Ebashi, S., and M. Endo. 1968. Calcium ion and muscle contraction. *Prog. Biophys. Mol. Biol.* 18:123–183.

Eisenberg, E., and L. E. Greene. 1980. The relation of muscle biochemistry to muscle physiology. *Annu. Rev. Physiol.* 42:293–309.

Ferenczi, M. A., E. Homsher, and D. R. Trentham. 1984. The kinetics of magnesium adenosine triphosphate cleavage in skinned muscle fibers of the rabbit. *J. Physiol. (Lond.).* 352:575–599.

Gillis, J. M., and G. Marechal. 1974. The incorporation of radioactive phosphate into ATP in glycerinated fibers stretched or released during contraction. *J. Mechanochem. Cell Motil.* 3:55–68.

Glyn, H., and J. Sleep. 1985. Dependence of adenosine triphosphatase activity of rabbit psoas muscle fibers and myofibrils on substrate concentration. *J. Physiol. (Lond.).* 365:259–276.

Goldman, Y. 1987. Kinetics of the actomyosin ATPase in muscle fibers. *Annu. Rev. Physiol.* 49:637–654.

Greene, L. E., and E. Eisenberg. 1980. Cooperative binding of myosin subfragment-1 to the actin-troponin-tropomyosin complex. *Proc. Natl. Acad. Sci. USA.* 77:2616–2620.

Hammes, G. G. 1968. Relaxation spectrometry of biological systems. *Adv. Protein Chem.* 23:1–57.

Herzig, J. W., and J. C. Rüegg. 1977. Myocardial cross-bridge activity and its regulation by Ca^{2+}, phosphate and stretch. *In* Myocardial Failure. G. Riecker, A. Weber, and J. Goodwin, editors. Springer-Verlag New York Inc., New York. 41–51.

Herzig, J. W., J. W. Peterson, R. J. Solaro, and J. C. Rüegg. 1982. Phosphate and vanadate reduce the efficiency of the chemo-mechanical energy transformation in cardiac muscle. *In* Regulation of Phosphate and Mineral Metabolism. S. G. Massry, J. M. Latteri, and E. Ritz, editors. Plenum Publishing Corp., New York. 267–281.

Hibberd, M. G., J. A. Dantzig, D. R. Trentham, and Y. E. Goldman. 1985*a*. Phosphate release and force generation in skeletal muscle fibers. *Science (Wash. DC).* 228:1317–1319.

Hibberd, M. G., M. R. Webb, Y. E. Goldman, and D. R. Trentham. 1985*b*. Oxygen exchange between phosphate and water accompanies calcium-regulated ATPase activity of skinned fibers from rabbit skeletal muscle. *J. Biol. Chem.* 260:3495–3500.

Homsher, E., and N. C. Millar. 1990. Caged compounds and striated muscle contraction. *Annu. Rev. Physiol.* 52:875–896.

Huxley, A. F. 1980. Reflections on Muscle. Princton University Press, Princeton, NJ. 93–95.

Inoue, A., T. Arata, and M. Yasui. 1989. Free energy change in the elementary steps of actomyosin ATPase reactions. *In* Muscle Energetics. R. J. Paul, G. Elzinga, and K. Yamada, editors. Alan R. Liss, Inc., New York. 15–26.

Kawai, M. 1982. Correlation between exponential processes and crossbridge kinetics. *In* Basic Biology of Muscles: A Comparative Approach. B. M. Twarog, R. J. C. Levine, and M. M. Dewey, editors. Raven Press, Ltd., New York. 109–130.

Kawai, M. 1986. The role of orthophosphate in crossbridge kinetics in chemically skinned rabbit psoas fibers as detected with sinusoidal and step length alterations. *J. Muscle Res. Cell Motil.* 7:421–434.

Kawai, M., and P. W. Brandt. 1980. Sinusoidal analysis; a high resolution method for correlating biochemical reactions with physiological processes in activated skeletal muscles of rabbit, frog and crayfish. *J. Muscle Res. Cell Motil.* 1:279–303.

Kawai, M., and H. R. Halvorson. 1989*a*. A crossbridge scheme in skinned rabbit psoas fibers deduced from relaxation kinetics and sinusoidal length perturbation analyses. *Biophys. J.* 55:260a. (Abstr.)

Kawai, M., and H. R. Halvorson. 1989*b*. Role of MgATP and MgADP in the crossbridge kinetics in chemically skinned rabbit psoas fibers. Study of a fast exponential process (C). *Biophys. J.* 55:595–603.

Kawai, M., R. N. Cox, and P. W. Brandt. 1981. Effect of Ca ion concentration on cross-bridge kinetics in rabbit psoas fibers. Evidence for the presence of two Ca-activated states of thin filament. *Biophys. J.* 35:375–384.

Kawai, M., K. Güth, K. Winnikes, C. Haist, and J. C. Rüegg. 1987. The effect of inorganic phosphate on the ATP hydrolysis rate and the tension transients in chemically skinned rabbit psoas fibers. *Pfluegers Arch. Eur. J. Physiol.* 408:1–9.

Kushmerick, M. J., and R. E. Davies. 1969. The chemical energetics of muscle contraction. II. The chemistry, efficiency and power of maximally working sartorius muscles. *Proc. R. Soc. Lond. Biol. Sci.* 174:315–353.

Levy, R. M., Y. Umazume, and M. J. Kushmerick. 1976. Ca^{2+} dependence of tension and ADP production in segments of chemically skinned muscle fibers. *Biochim. Biophys. Acta.* 430:352–365.

Lund, J., M. R. Webb, and D. C. S. White. 1987. *J. Biol. Chem.* 262:8584–8590.

Lymn, R. W., and E. W. Taylor. 1971. The mechanism of adenosine triphosphate hydrolysis by actomyosin. *Biochemistry.* 10:4617–4624.

Molloy, J. E., V. Kyrtatas, J. C. Sparrow, and D. C. S. White. 1987. Kinetics of flight muscles from insects with different wingbeat frequencies. *Nature (Lond.).* 328:449–451.

Meyer, R. A., T. R. Brown, and M. J. Kushmerick. 1985. Phosphorus nuclear magnetic resonance of fast- and slow-twitch muscle. *Am. J. Physiol.* 248:C279–C287.

Nagano, H., and T. Yanagida. 1984. Predominant attached state of myosin cross-bridges during contraction and relaxation at low ionic strength. *J. Mol. Biol.* 177:769–785.

Nonomura, Y., E. Katayama, and S. Ebashi. 1975. Effect of phosphate on the structure of the actin filament. *J. Biochem. (Tokyo).* 78:1101–1104.

Nosek, T. M., K. Y. Fender, and R. E. Godt. 1987. It is diprotonated inorganic phosphate that depresses force in skinned skeletal muscle fibers. *Science (Wash. DC).* 236:191–193.

Pate, E., and R. Cooke. 1989. Addition of phosphate to active muscle fibers probes actomyosin states within the power stroke. *Pfluegers Arch. Eur. J. Physiol.* 414:73–81.

Rüegg, J. C., M. Schädler, G. J. Steiger, and G. Müller. 1971. Effects of inorganic phosphate on the contractile mechanism. *Pfluegers Arch. Eur. J. Physiol.* 325:359–364.

Schoenberg, M. 1988. Characterization of the myosin adenosine triphosphate (M · ATP) crossbridge in rabbit and frog skeletal muscle fibers. *Biophys. J.* 54:135–148.

Siemankowski, R. F., M. O. Wiseman, and H. D. White. 1985. ADP dissociation from actomyosin subfragment 1 is sufficiently slow to limit the unloaded shortening velocity in vertebrate muscle. *Proc. Natl. Acad. Sci. USA.* 82:658–662.

Sleep, J. A., and R. L. Hutton. 1980. Exchange between inorganic phosphate and adenosine 5′-triphosphate in the medium by actomyosin subfragment 1. *Biochemistry.* 19:1276–1283.

Stein, L. A., R. P. Schwarz, P. B. Chock, and E. Eisenberg. 1979. Mechanism of actomyosin adenosine triphosphatase. Evidence that adenosine 5′-triphosphate hydrolysis can occur without dissociation of the actomyosin complex. *Biochemistry.* 18:3895–3909.

Takashi, R., and S. Putnam. 1979. A fluorimetric method for continuously assaying ATPase: application to small specimens of glycerol-extracted muscle fibers. *Analyt. Biochem.* 92:375–382.

Taylor, E. W. 1979. Mechanism of actomyosin ATPase and the problem of muscle contraction. *CRC Crit. Rev. Biochem.* 6:103–164.

Taylor, E. W. 1986. Mechanism and energetics of actomyosin ATPase. *In* The Heart and Cardiovascular System. H. A. Fozzard, E. Haber, R. B. Jennings, and A. M. Katz, editors. Raven Press, Ltd., New York. 789–802.

Tonomura, Y., H. Nakamura, N. Kinoshita, H. Onish, and M. Shigekawa. 1969. The pre-steady state of the myosin-adenosine

triphosphate system. X. The reaction mechanism of the myosin-ATP system and a molecular mechanism of muscle contraction. *J. Biochem. (Tokyo).* 66:599–618.

Ulbrich, M., and J. C. Rüegg. 1971. Stretch induced formation of ATP-^{32}P in glycerinated fibres of insect flight muscle. *Experimentia (Basel).* 27:45–46.

Ulbrich, M., and J. C. Rüegg. 1977. Mechanical factors affecting the ATP-phosphate exchange reaction of glycerinated insect fibrillar muscle. *In* Insect Flight Muscle. R. T. Tregear editor. North-Holland Biomedical Press, Amsterdam, The Netherlands. 317–333.

White, H. D., and E. W. Taylor. 1976. Energetics and mechanism of actomyosin adenosine triphosphatase. *Biochemistry.* 15:5818–5826.

White, D. C. S., and J. Thorson. 1972. Phosphate starvation and the nonlinear dynamics of insect fibrillar flight muscle. *J. Gen. Physiol.* 60:307–336.